Rapid learning and integration of artificial sensation

Samuel Senneka and Maria C. Dadarlat*

Weldon School of Biomedical Engineering, Purdue University, West Lafayette, IN * corresponding author: mdadarla@purdue.edu

1 Summary

Prosthetic limbs lack proprioceptive feedback, which is essential for complex movements. Intracortical microstimulation (ICMS) elicits sensory perceptions that could serve as an artificial proprioceptive signal. However, movements guided by ICMS are slower and less accurate than those with natural sensation. Here, we developed a freely-moving mouse behavioral task to improve ICMS encoding of artificial sensation. Mice implanted with 16-channel microwire arrays in primary somatosensory cortex were trained to navigate to targets upon the floor of a custom behavioral training cage. Target location was encoded with visual and/or ICMS feedback. Mice quickly learned to use the ICMS signal to locate invisible targets, achieving 75% proficiency on ICMS-only trials by the first three sessions of testing. Furthermore, performance on multimodal trials significantly exceeded unimodal performance, demonstrating that animals integrated natural vision with artificial sensation. This protocol can be applied to efficiently develop and test algorithms to encode artificial proprioception for neural prostheses.

2 Introduction

The native human somatosensory system has access to an array of complex, dynamic inputs whose informational content is constructed from the activation of sensors distributed throughout the body [1]. The neural circuits underlying somatosensory processing remain remarkably plastic into adulthood, rapidly adapting to the statistics of sensory inputs: expanding the somatotopic representation of task-relevant information from the fingertips [2], developing novel multisensory responses to paired multimodal stimuli [3], and shifting receptive fields to incorporate extracorporeal objects such as tools [4]. Similarly, cortical neurons plastically adapt their response properties when directly activated by small, local electrical currents (intracortical microstimulation; ICMS): expanding local somatotopic representations [5], altering functional connectivity between neurons [6], and shifting neural projection fields [7]. Humans and animals can perceive neural activity elicited by electrical stimulation [8–12], making ICMS a promising tool for encoding artificial sensation to replace lost sensory function [13, 14] or to provide closed-loop feedback for neural prostheses such as Brain-Machine Interfaces (BMIs; e.g., [15]).

Animals learn to detect and interpret distinct spatial and temporal patterns of electrical stimulation across an array of electrodes, ultimately using multi-channel ICMS to guide perception and movement [11, 16–24]. This is particularly important for BMIs, which establish an artificial sensorimotor system that uses sensory information to modulate neural activity that to control the movement of a computer cursor or robotic arm [25–29]. Currently, BMI patients primarily rely on visual feedback of the prosthetic to guide movements; in contrast, humans rely on both visual and proprioceptive feedback to estimate hand position during reaching [30]. When multiple sensory representations of a single variable are available, they are combined into a unified, and more precise, sensory estimate in a process called multisensory integration [31]. Multisensory integration facilitates and improves sensory-guided perception and behavior [32] and will therefore be a critical component of artificial sensorimotor function such as BMIs. Nevertheless, movements guided by artificial sensation have so far failed to be as direct and precise as those guided by natural sensory signals. Furthermore, the scale of information that has been encoded is yet limited — usually a single sensory variable. The major questions from the perspective of encoding artificial sensation then are: 1) how to encode sensory information precisely, 2) how to encode multiple variables, and 3) what are the requirements for artificial sensation to be integrated with natural sensory information?

To address these questions, we developed a rapid and robust protocol by which to study learning and integration of artificial sensation in freely moving mice. Using this protocol, we tested the hypothesis that artificial information would be integrated with natural vision even when the two sensory streams were encoded in distinct frames of reference. We showed that artificial sensation can be integrated with natural vision even

though ICMS encoded target location in ego-centered polar coordinates (distance and direction of the target relative to the head) while vision encoded a *static* target location in retinotopic space (a fixed location upon the cage floor). The learning of artificial sensation was rapid and robust across animals, and the timeline for learning to integrate natural and artificial sensation matched the timeline for learning the artificial sensory signal itself. These results demonstrate the surprising flexibility of neural circuits in adapting to and integrating novel (artificial) forms of sensory information, which is an important consideration in the development of brain-computer interfaces.

3 Results

Five C57BL/6J mice were trained to navigate to a 2 cm target located on the floor of a custom behavioral training cage (Suppl. Figure 1A). The target could be set to one of nine possible locations, forming a three by three grid upon the cage floor (Suppl. Figure 1B). The target location was made known to the mice via two sensory modalities: 1) vision (a circle upon the floor), and/or 2) multi-channel ICMS. The ICMS signal encoded a two-dimensional vector specifying 1) the angle between the mouse's heading and the target (θ) and 2) the distance between the mouse's head and the center of the target (δ; Figure 1B). The ICMS signal encoding of target location was designed to imitate the known encoding of limb movements in primary somatosensory cortex, which are thought to take the form of a "movement vector" describing the distance and direction of a limb movement [33–35] (Figure 1A). To reduce the saliency of the visual target, it was dim (6 lux) and red (630 nm). Although mice are dichromats (they have no red cones in the retina), they are not blind to red light [36]. During each trial, the mouse's head and body (Figure 1F) were tracked using DeepLabCut Live on a 60 Hz video feed from a camera mounted on the top of the behavioral training cage [37]. A behavioral trial was considered successful if the mouse's head entered the target during a 5-10 s trial period.

Encoding multi-variate artificial sensation.

The artificial sensory signal was encoded via spatiotemporally patterned ICMS (Figure 1D-F). The basic unit of electrical stimulation is a biphasic pulse of current (Figure 1D), and the effect of stimulation on nearby neurons depends on the parameters used for stimulation, including the current amplitude, location of stimulation, and the frequency at which pulses are delivered [9, 38–42]. The ICMS signal was designed to imitate neural encoding of natural proprioception (Figure 1A,B). Each electrode was assigned a tuning curve in the form of a von Mises distribution centered on a "preferred direction" (*phi*) (Figure 1D; [33, 34]), equally spaced around a circle from 0 to 2π (Figure 1E). The direction of the target relative to the mouse's heading could be decoded from the relative stimulation frequencies across electrodes (Figure 1D,F). The distance between the mouse's head and the center of the target (δ) scaled the amplitude of the tuning curve (maximum stimulation frequency; Figure 1E). To maintain a robust signal at all distances, electrodes were split into "proximal" and "distance" groups. The proximal group tuning curves were scaled by $(1-\delta/\delta_{max}))$, increasing average stimulation frequency as the mouse approached the target. The distance group were scaled by (δ/δ_{max}), decreasing stimulation frequency as the mouse approached the target. The distance between the target and the mouse's head could therefore be decoded from the ratio of stimulation frequencies between the proximal and distance electrodes (Figure 1E,F).

Learning to interpret artificial sensory information.

Animals received multimodal sensory information (both visual and ICMS encoding of target location) from the first day of training on the behavioral task. All five mice quickly learned the multimodal behavioral task (Figure 2A), locating the target on at least 75% of trials within the first seven days of training [43]. Further training did not improve performance, as task completion on the last three days of testing was not statistically different from the first three days following proficiency ($p \geq 0.05$, Wilcoxon rank-sum test, Figure 2B). In both early and late sessions, task completion was significantly better than the threshold set for proficiency (75%; $p \leq 0.05$, t-test). Therefore, animals quickly learn and stabilize performance on this behavioral task.

Once an animal's behavioral performance reached high accuracy (75%), we introduced a series of probe trials intended to test learning and integration of the ICMS signal. To test learning of the ICMS signal, ICMS probe trials were presented on $7.5-15\%$ of trials per session. In these trials, the target location was

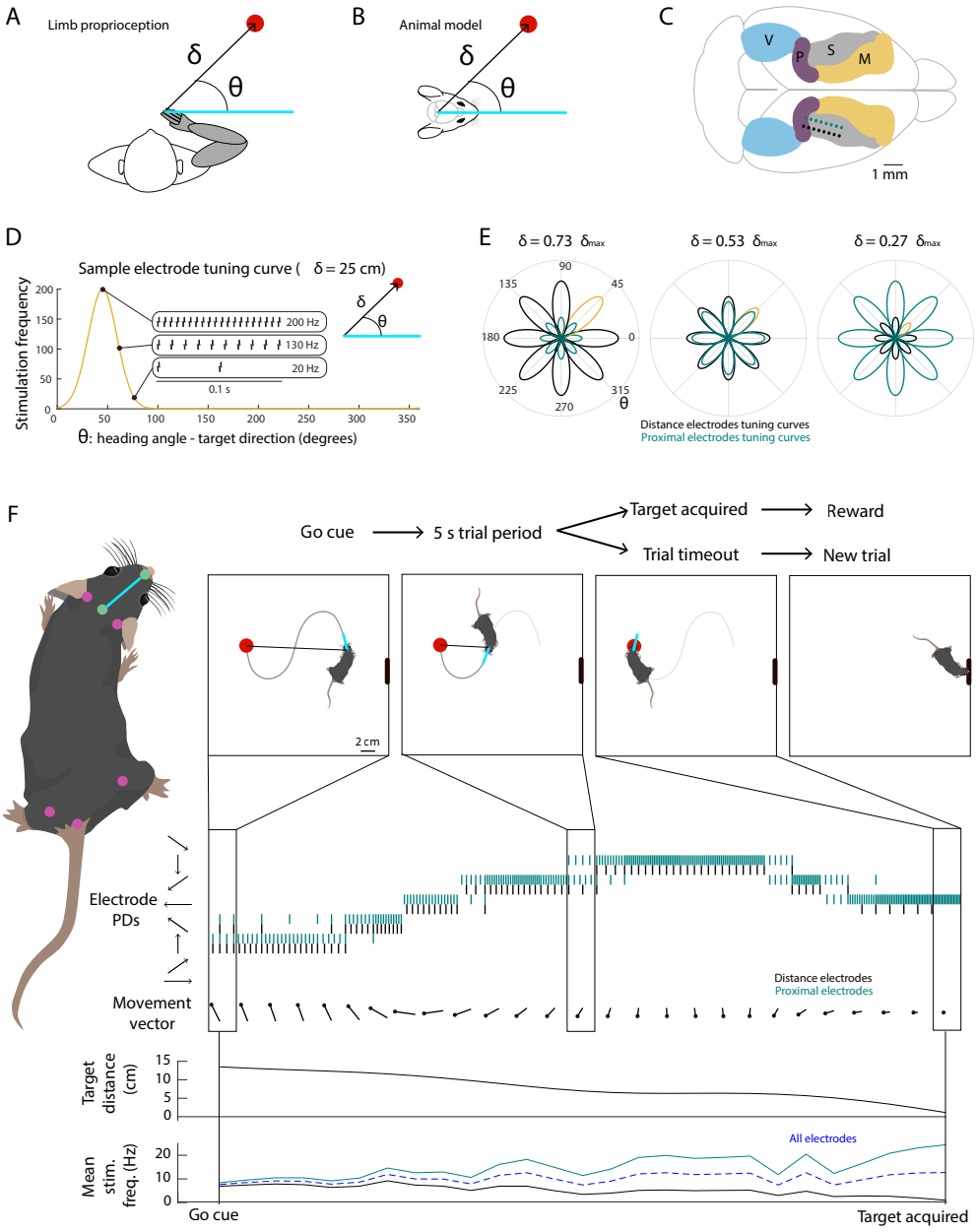

Figure 1: Encoding multi-variable artificial sensation via spatiotemporal patterned electrical microstimulation. **A.** Artificial sensation from a prosthetic limb encodes the distance (δ) and direction (θ) of movements. **B.** Animal model for artificial sensation: ICMS encodes the distance (δ) and direction (θ) between the animal's heading and a rewarded target location. **C.** A sixteen-channel microwire array is implanted unilaterally over mouse primary somatosensory cortex (S), anatomically close to parietal (P), motor (M), and visual (V) cortices. **D.** Sample single electrode tuning curve shows stimulation frequency as a function of θ for fixed δ. **E.** Tuning curves for all sixteen electrodes as a function of target distance (δ) for distance (black) and proximal (green) electrodes. The yellow tuning curve shows the sample electrode in (C). **F.** A simulated behavioral trial, showing animal heading and movement trajectory (top). Left: animal pose is tracked in real-time within the cage (pink and green dots). Pose is used to calculate heading direction (vector between the nose and midpoint between the ears). Heading direction is used to calculate δ and θ. Stimulation parameters are updated at 10 Hz. Right: simulated stimulation patterns across "proximal" and "distance" group electrodes as a function of the movement vector across time (s).

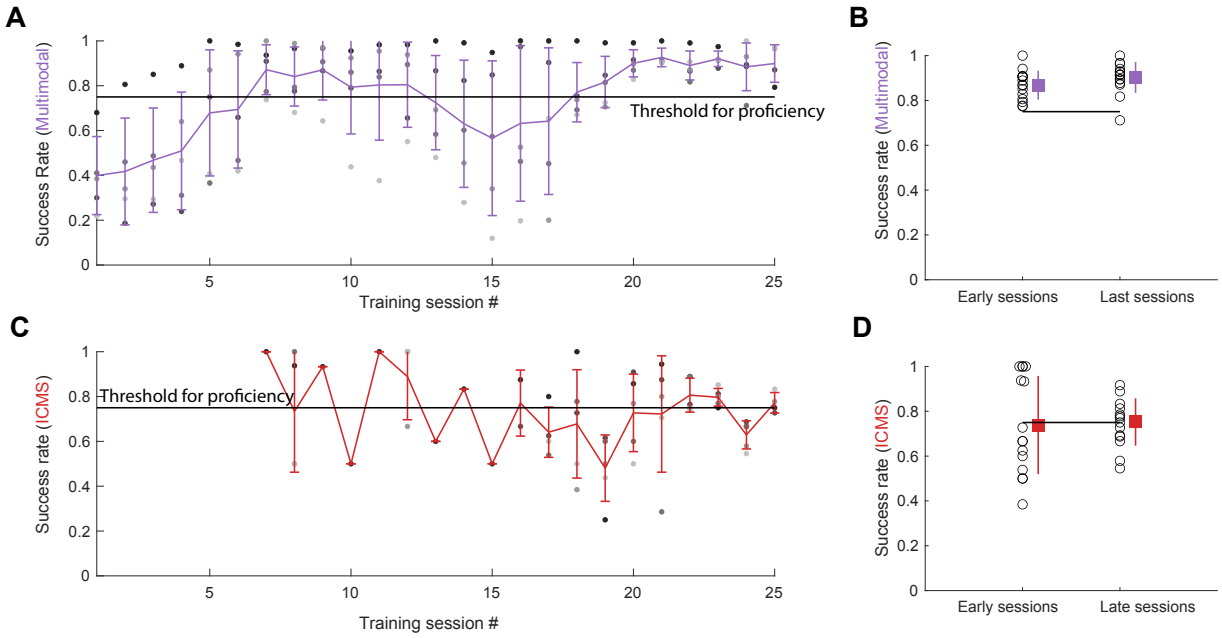

Figure 2: Learning to interpret artificial sensation. **A.** Average single-day success rates on multi-modal trials for each mouse (colored circles). The purple trace shows the daily mean and standard deviation across animals. The noticeable dip around days 14-18 reflects poor performance after a break in training (day 13). **B.** Average success rates on multimodal trials for all mice on the first three days of task proficiency vs. the last three days of training. The gray line represents the 75% threshold for proficiency. There is no significant difference between between early/late success rates ($p \geq 0.05$, Wilcoxon sign-rank test). **C.** Average single-day success rates on ICMS trials for each mouse (colored circles). The red trace sows the daily mean and standard deviation across animals. Not all mice were tested in each session. **D.** Analysis as in (B) for ICMS trials. There is no significant difference between early/late success rates ($p \geq 0.05$, Wilcoxon sign-rank test).

invisible to the mouse. We included vision-only probe trials that could have dim or bright visual target trials in order to compare natural and artificial sensation ($7.5 - 15\%$ and $2.5 - 5\%$ of trials). Probe trials also included a sham condition, where no sensory information was provided about target location and therefore showed success rates possible by chance (2.5 - 5%).

While day-to-day performance on ICMS trials fluctuated, animals had relatively stable performance on ICMS trials, fluctuating around the 0.75% level set for proficiency (Figure 2C). Furthermore, success rates for ICMS trials were similar between early and late training sessions (Figure 2D). From these analyses, we conclude that animals quickly learn to decode task-relevant sensory information from the ICMS signal and that decoding is stable across time. To quantify behavioral performance beyond success rate, we also calculated per-trial path efficiency and time-to-target using the last five behavioral sessions per mouse.

Mice clearly learned to use the ICMS signal to locate the invisible targets within the training cage. In fact, behavioral performance guided by ICMS was qualitatively (Figure 3B) and quantitatively (Figure 3C-F) similar to behavioral performance when navigating to dim and bright visual targets ($p \geq 0.05$, Wilcoxon rank sum test). Under all sensory conditions, mice completed significantly more trials than chance, suggesting that mice are making directed movements towards the target on all trial types ($p \leq 1e - 5$; Wilcoxon rank sum test, Bonferroni correction for multiple comparisons).

Integration of natural and artificial sensation.

We hypothesized that, if natural visual information were being integrated with artificial sensory information, behavioral performance on multimodal trials would be significantly better than on unimodal trials. This seems to be case (Figure 3A,C-F). Mice completed significantly more trials and made faster and more efficient movements in multimodal than unimodal trials (Figure 3C,D,E). Integration matches the timeline for learning the ICMS signal: by the time unimodal probe trials were tested, animals were already integrating ICMS with vision (Figure 3F). While there is prior evidence of multisensory integration of natural and artificial sensation [15, 22, 44, 45], our current work highlights the speed and flexibility by which integration is learned. Specifically, we show here that the signals are integrated even when there is a mismatch in the reference frames in which sensory information is encoded (Figure 3A).

Decoding of direction and distance variables from ICMS. Given that the artificial sensory signal encodes two variables (Figure 1B), we next asked how well the animals could decode each (distance and direction) from ICMS. This question is challenging to address given the circuitous trajectory taken by the animals even to bright visual target trials (Figure 3B). Therefore, we used behavioral performance on bright visual trials to estimate the intrinsic variability of mouse trajectories. Additional variability could then be assigned to an inability to extract task-relevant information about target location.

To estimate decoding of movement angle and distance from the ICMS signal, we separated single-trial movement trajectories into discrete sub-movements based on changes in velocity [46]. The distinct sub-movements allows us to quantify changes in heading and distance relative to the target in response to sensory information available at the onset of the movement (Figure 4A). At the onset of movement, the mouse is at some location (θ_{onset}, δ_{onset}) relative to the target (Figure 4A, top left). If the animal can perfectly decode both direction and distance from the ICMS signal, an optimal movement would take the animal directly to the target, such that $\theta_{offset} = 0$ (equally, $\theta_{onset} - \theta_{offset} = \theta_{onset}$) and $\delta_{offset} = 0$. No movement would lead to $\theta_{onset} - \theta_{offset} = 0$ and $\delta_{offset} = \delta_{onset}$. Only trials in which distinct sub-movements could be identified were included in this analysis ($\sim 50\%$ of trials).

Onset target angle (θ_{onset}) and change in θ during the sub-movements were significantly correlated across trial types ($p \leq 0.001$, significance of F-statistic for linear regression (not shown); Figure 4B). This suggests that mice were able to extract target direction information from all evaluated sensory inputs, including artificial sensation encoded by ICMS. In contrast, estimations of target distance were only accurate on multimodal and ICMS trials ($p \leq 0.001$, significance of F-statistic in linear regression (not shown); Figure 4C). This suggests that mice followed a different kinematic strategy during visual trials than during multimodal and ICMS trials.

We also used two indirect measures to test the hypothesis that ICMS accurately encodes distance and direction. First, we noted that mice "faced" the bright visual target for an average of 78% of the trial (Figure 4D), defined as the fraction of time the target is within the mouse's field of view [47]. Similarly, mice faced the target 75% of the time when guided by ICMS — nearly identical to the 74.5% of the time when guided by the dim visual signal, and not significantly different from facing time in bright visual trials. In

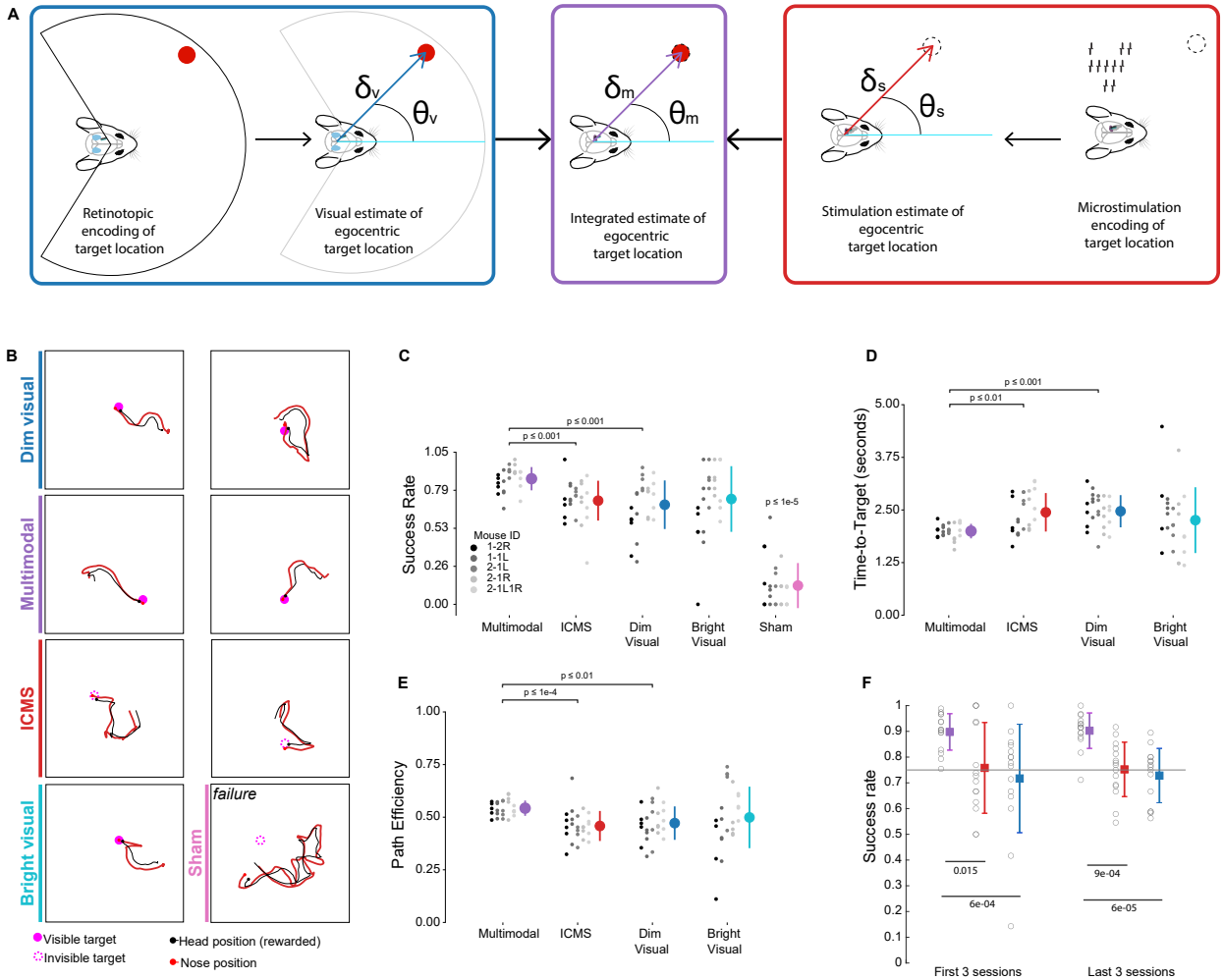

Figure 3: Integration of natural and artificial sensation. **A.** Computational requirements for multisensory integration of natural vision with artificial ICMS-based sensory encoding (δ_m,θ_m) includes combining visual estimates of distance and direction (δ_v,θ_v) with those estimated from the ICMS signal (δ_s,θ_s). **B.** Sample single-trial trajectories for each trial type. **C.** Success rate (fraction of the time that the target was localized within the five second window). **D.** Average trial duration (from the go cue to target acquisition) **E.** Path efficiency (direct path relative to total path length). **F.** Success Rate over early sessions (first three sessions of proficiency) vs. late sessions (last three sessions).

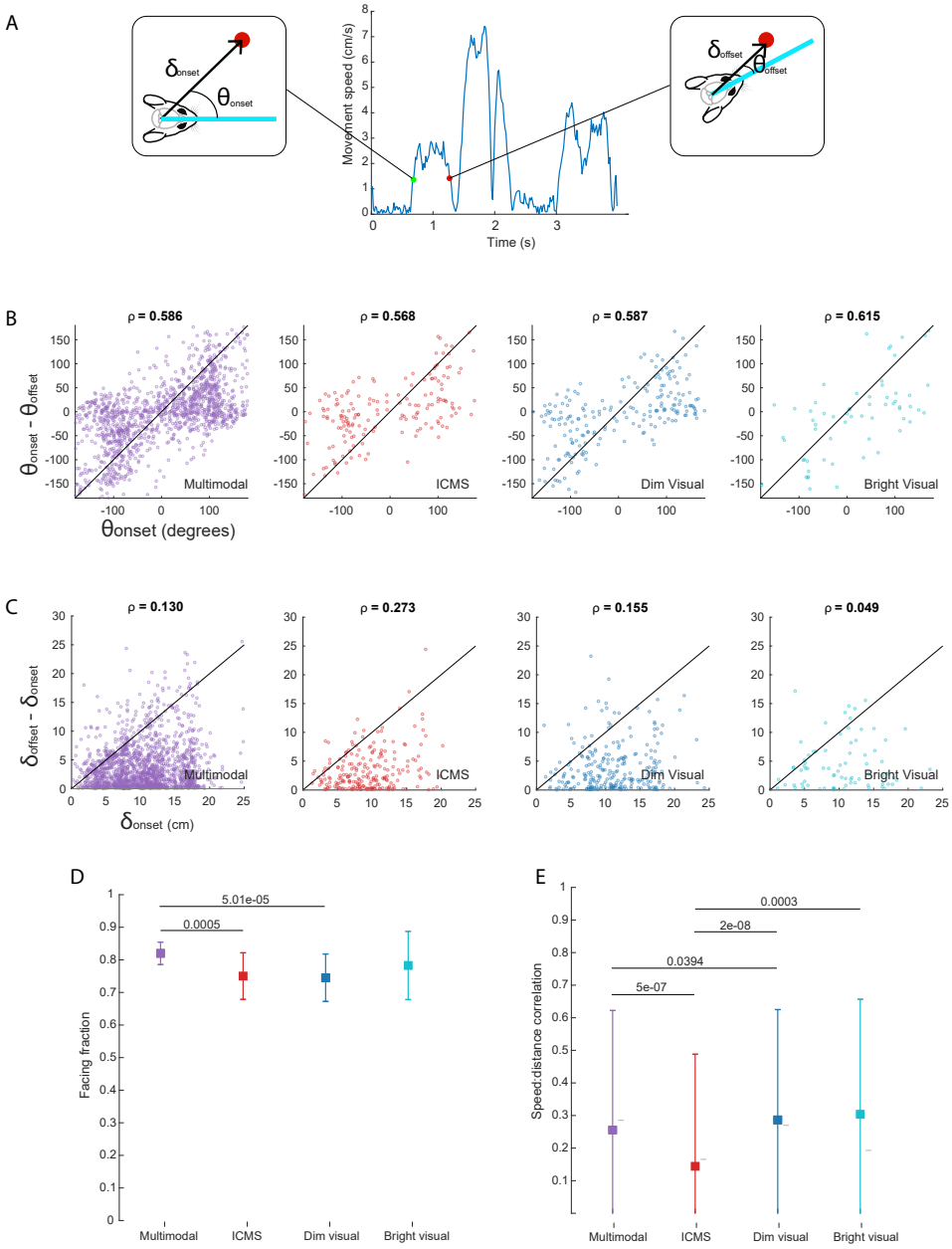

Figure 4: Estimation of relative target angle and distance from the ICMS signal. **A.** Example of identifiable sub-movements from the absolute radial speed of the mouse on a single trial. We use the first sub-movement after the start of the trial to infer the animal's estimate of the direction (θ) and distance (δ) between it's head and the target at the beginning of the sub-movement. Angle estimation is inferred from the change in angle between sub-movement onset (θ_{onset}) and sub-movement offset (θ_{offset}). Similarly, distance estimation is inferred from the change in distance between sub-movement onset (δ_{onset}) and sub-movement offset (δ_{offset}). Data comes all five mice. **B.** Decoding θ on each trial type. Each circle represents the first sub-movement of a single trial. for trials that show this stereotyped behavior. The black diagonal line represents unity. ρ represents the correlation between the true angle at the beginning of the sub-movement (θ_{onset}) and the estimated angle inferred from the sub-movement ($\theta_{onset} - \theta_{offset}$). **C.** Decoding of δ on each trial type. Circles and lines as in (B). ρ represents the correlation between the true distance at the beginning of the sub-movement (δ_{onset}) and the estimated distance inferred from the sub-movement ($\delta_{offset} - \delta_{offset}$). **D.** Fraction of each trial spent facing the target is used to indirectly infer the animals's ability to calculate relative target angle, θ, across trials types. Facing is defined as having a heading relative to the target of less than 123° in either direction. P-values show statistically significant differences in facing between trial types using a Wilcoxon rank-sum test. **E.** Single-trial correlations between movement speed and distance to the target is used to indirectly infer the mouse's ability to calculate relative distance, δ, across trials types. P-values show statistically significant differences in facing between trial types using a Wilcoxon rank-sum test.

contrast, on multimodal trials, mice faced the target an average 82% of the time – significantly more than on ICMS or dim visual target trials ($p = 5e-4$ and $p = 5e-5$ respectively; Wilcoxon rank-sum test). This facing measure thus further supports the assertion that ICMS and visual information are integrated during behavior.

Second, we noted that mice slowed down as they approached the bright visual target, reflected by a positive correlation between target distance and movement speed ($\rho = 0.30$; Figure 4E). This behavior may reflect the well-known trade-off between the speed and accuracy of movements (Fitt's law), suggesting that movements become slower and more precise as the animal knowingly approaches the target. Similarly, target distance and movement speed were positively correlated for ICMS trials ($p = 8e-27$, t-test). However, the correlation between target distance and movement speed was lower for ICMS trials than for either dim visual trials or bright visual trials ($p = 2e-8$ and $p = 3e-4$, Wilcoxon rank sum test), suggesting that distance information from the ICMS signal was not encoded as well as the visual signal.

4 Discussion

Our major finding is that freely-moving animals quickly learn to both decode and integrate multi-variate artificial sensation encoded by patterned ICMS. Animals learned to decode direction, and to a lesser extent, distance, from an ICMS signal, with accuracies comparable to natural vision. Integration of natural vision with artificial sensation occurred even though the two signals were encoded in two distinct frames of reference: the visual target appeared as a red circle centered at some (x,y) position upon the cage floor, while the ICMS signal directly encoded position in polar coordinates (θ,δ). That the two signals were nevertheless integrated emphasizes the flexibility of the nervous system in processing and adapting to novel forms of sensory information, including integrating information that is not available via natural sensors. Finally, we showed that the timeline of integration tracks the timeline of learning the ICMS signal, suggesting that integration is a natural consequence of learning in the context of sensory-guided behavior [48]. We propose that this protocol may be used to rapidly study the optimal methods for multi-variate encoding of artificial sensation.

Artificial proprioceptive information is required for precise control of a robotic limb.

Artificial proprioceptive feedback from a prosthesis should encode the position and movement of the limb through space [1]. A major engineering challenge is thus to encode as many sensory variables as possible (feedback from the shoulder, elbow, hand, fingers, etc.) with as few electrodes as possible (e.g., 100 in the Utah array [49]). Therefore, refining algorithms used to encode artificial sensation to improve its reliability and precision is a critical area of research. Previous work in freely-moving rodents has demonstrated speed of learning of ICMS in this context, suggesting that this model is ideal for early development of encoding strategies for artificial sensation [18, 19, 50–52].

How much learning is necessary for artificial sensation?

An informal distinction in the field of artificial sensation is whether or not neuromodulation is "biomimetic." This term conveys the idea that an optimal form of artificial sensation is one that takes no learning, by which electrical stimulation can directly replace natural sensation in the context of behavioral perception and discrimination (e.g., [10, 12]). Intuitively, the nervous system is optimized to interpret and generate specific activity patterns, and movement away from those patterns requires neural plasticity[53–55]. Consequently, understanding how electrical stimulation can be patterned to evoke neural activity patterns similar to those induced by natural sensation is a major concern [56–58]. These efforts have been particularly successful in the field of artificial touch, where neurons have readily-identifiable receptive fields and electrical stimulation induces sensation on clearly demarcated parts of the body [8, 9, 11].

Achieving similar results for artificial proprioception is challenging, due to the complexity of the proprioceptive neural code [33–35] (but see [59, 60]). In general, any finite number of electrodes is unlikely to be able to precisely access and modulate neurons with all of the desired encoding properties [59]. Therefore, encoding the full range of artificial proprioceptive signals from even a single limb will require some level of learning from the subject [61]. Our approach investigates an extreme circumstance: what if almost *everything* has to be learned? Addressing this question sets a lower bound for behavior guided by electrical stimulation and demonstrates the extent to which learning and plasticity can be engaged by neural prostheses. That said, as mentioned in the text, our design of stimulation patterns was inspired by observations regarding

natural neural encoding of proprioception, which may be an important consideration for encoding artificial proprioception.

5 Methods

5.1 Mice

All procedures were approved by the Institutional Animal Care and Use Committee at Purdue University. Five C57BL/6J mice (Jackson Labs #000664) aged 3-4 months were used in these experiments (4 males, 1 female). Mice were housed in groups of no more than five per cage in a temperature and humidity-controlled room on a 12-hour light/dark cycle with *ad libitum* access to food and water prior to surgery. Mice were single-housed following surgery for the duration of the experiments. During training, mice had free access to citric acid water (0.5-5%) within their home cages [62]. In the behavioral training cage, mice received a 0.1 mL strawberry Nesquik reward for each successful trial.

5.2 Surgical Procedures

Each mouse underwent a chronic microwire array implantation surgery prior to behavioral training. 16-channel microwire arrays (TDT OMN1010-16) were implanted over the forelimb/hindlimb region of mouse primary somatosensory cortex. This region was identified using stereotaxic coordinates (Paxinos and Franklin's the Mouse Brain in Stereotaxic Coordinates).

To prepare for surgery, each was induced to anesthesia using 1-3% isoflurane and maintained at 1-2% to areflexia. Ophthalmic ointment was applied to each eye. Mice were then given subcutaneous doses of meloxicam (10 mg/kg) and dexamethasone (100 mg/kg) prior to the start of surgery. Next, 0.2% lidocaine (.03 mL) was injected cutaneously on the scalp and the scalp was resected.

Prior to electrode array implantation, a ∼1 x 2.5 mm craniectomy was made in the right hemisphere over the posterior portion of primary somatosensory cortex and the anterior portion of posterior parietal cortex. Electrode arrays consist of 16-channel microwire arrays in an 8x2 layout. Each electrode is 2 mm long. Within each row of the array (8 electrodes), electrodes are spaced 250 μm apart, and the two rows are 500 μm apart. Electrode arrays were implanted to a depth of 500 μm using a digital stereotax (Stoelting). Following array implantation, a thin layer of silicone elastomer (KwikSil) was used to cover the exposed brain, and the array was secured to the skull with dental cement (Metabond).

To implant ground ad reference wires, two burr holes were created in the contralateral hemisphere. Using these burr holes, silver ground and reference wires were implanted just underneath the skull. On three of the animals, a two mm 0-80 screw was also placed in the temporal ridge contralateral to implantation site to secure the implant. Additional dental cement was applied to secure the array, ground and reference wires, and screw.

Mice were treated post-operatively with meloxicam (10 mg/kg) and dexamethasone (100 mg/kg) for three and seven days post-op, respectively, and were given five to seven days to recover before training began.

5.3 Behavioral training

Behavioral training chamber The behavioral task required mice to locate a target that could appear in one of nine locations upon the floor of the behavioral training chamber. The chamber was a custom-designed and fabricated rectangular chamber (24 cm x 25.4 cm) made of acrylic with a clear floor (Suppl. Figure 1A). Visual targets were generated using a 32x32 LED RGB matrix with a pitch of 6 mm (Adafruit Product ID: 1484) placed just underneath the cage floor. Visual targets were generated by turning on groups of LEDs using red light (630 nm) with an intensity of 6 and 30 lux for dim and bright targets respectively. A reward port was placed upon the center of one wall, approximately 2 cm off the ground (Suppl. Figure 1A). Two speakers (what kind) were mounted on opposing walls to provide auditory cues, include a start tone (20 kHz, 0.5 s duration) and a reward tone (8 kHz, 1 s duration). Neural stimulation and recordings were performed using a Ripple Neuro Grapevine processor and Ripple Neuro pico+stim headstage. The mouse's position within the cage was recorded at 60 Hz with a camera mounted onto the top of the training chamber (Imaging Source monochrome camera DMK 37BUX287 used with an Imaging Source TPL 0420 6MP Lens).

We used a trained DeeplabCut pose estimation model and the DeepLabCut-Live GUI to track the mouse's movement on the real-time camera feed. A custom python processor script was used in conjunction with DeepLabCut-Live to randomly select target regions, provide reward, and update stimulation parameters during trials.

Habituation Animals were placed on 0.5-5% citric acid water within their homecage [62] and were habituated to the behavioral training chamber for three days prior to the start of behavioral training. Habituation consisted of 5-15 minutes sessions. During the habituation sessions, a reward port (Sanworks Product ID: 1009) was activated for a portion of every minute, alternating between an activation period (55 s) and a deactivation period (5 s). Reward port activation was indicated by a white LED on the port being illuminated and a tone being played at the onset of activation (1 second 8 kHz pure tone). If the mouse nose-poked the reward port during the 55 second activation period, the solenoid on the port was opened for 10 ms, delivering a drop of strawberry Nesquik. Subsequent nose-pokes did not provide reward until next activation period. Therefore, mice could receive a reward once every 60 s during habituation.

Training Subjects were initially trained to navigate to multimodal targets. To make the trials easy to complete, the dim visual targets were large (7-9 cm diameter) and the trial duration was long (10-12 s). As subjects completed approximately ≥80% of trials on each condition, target size and trial duration were gradually reduced to the final values of 2 cm diameter visual targets and 5 second trials. The training process took approximately four session, using consistent decreases in target diameter of 2 cm/session and 1-2 seconds/per session.

Testing Once mice performed well ($\geq$ 70% success rates) on multimodal trials, four additional trial types were introduced: ICMS-only, visual-only (dim and bright), and sham (no visual or ICMS). ICMS-only explicitly tests decoding of the artificial sensory signal, sham trials test success rates that are achievable by chance (setting a lower bound on performance), and the visual trials test baseline behavioral guided by unimodal natural feedback when the signal is highly reliable (bright visual) or less reliable (dim visual). The first two mice were tested using a trial probability distributions of 80% multimodal, 7.5% ICMS only, 7.5% dim visual only, 2.5% bright visual only, and 2.5% sham. To gain a more precise estimate of unimodal behavior, three subsequent mice were tested using a trial probability distributions of 60% multimodal, 15% ICMS only, 15% dim visual only, 5% bright visual only, and 5% sham.

5.4 Intracortical Microstimulation

ICMS pulses were cathode-leading biphasic symmetric pulses with a phase length of 200 μs and interphase interval of 250 μs with a constant amplitude of 10-20 μA. The frequency and location of stimulation were used to encode the vector describing the relative position between the mouse's forward heading and the target. For electrode i, stimulation frequency at time t was set to

$$f_i(t) = \delta_{rel}(t) * (200/e^{\kappa}) * e^{\kappa * cos(\phi_i - \theta(t))},$$

where $\theta(t)$ is the target direction relative to the animal's heading, ϕ_i is fixed for each electrode, $\delta(t)$ scales with distance to the target, and $200/e^{\kappa}$ scales the curves to a maximum stimulation frequency of 200 Hz. $\delta(t)$ was modeled as $\delta_{rel}(t) = \delta(t)/\delta_{max}$ and $\delta_{rel}(t) = 1 - \delta(t)/\delta_{max}$ for distal and proximal encoding electrodes, respectively, with $\delta_{max} = 26.5cm$ (diagonal distance across cage). Electrodes 1-8 (row 1) were set to be proximal encoding electrodes and electrodes 9-16 (row 2) were set to be distance encoding electrodes. Both electrodes located within each column of the 8 x 2 array had the same ϕ_i, a value that acted as a "preferred direction" for the electrodes as it is the direction at which the electrode had the highest stimulation frequency for fixed δ.

5.5 Analysis

Statistics Statistical analyses for unpaired samples were all performed using t-test or Wilcoxon rank sum test and corrected for multiple comparisons using the Bonferroni correction. Paired samples (such as comparing behavior of a single mouse on different trial types each day) were tested using the Wilcoxon sign-rank test.

Behavioral analysis Trajectories taken during trials were cleaned prior to analysis due to noise in the DeepLabCut tracking algorithm. This cleaning was achieved by identifying timepoints with low probability

of being correct (a measure provided by DeepLabCut) and averaging the value of the two surrounding, higher-probability points.

Trial cropping. On a subset of trials, the mouse is not originally facing the target. To ensure a fair comparison between visual and ICMS trials, we cropped behavioral trajectories on each trial to the point at which the mouse is first facing the target, defined as the point at which the mouse heading (vector between the nose and back of the head; Figure 1) is within $\pm 123^o$ of the target direction, δ. Subsequent trial metrics (described below) were calculated using these cropped trajectories. We then quantified behavioral performance under each sensory condition with three behavioral measures: success rate, path efficiency, and time-to-target.

Path efficiency is calculated as the ratio between the direct distance to the target at beginning of the trial and the total path length traveled by the animal during the trial. The total path length is calculated by taking the point-wise difference in x and y-positions across the time, converting those differences into polar coordinates (r, θ), and adding all r between the start and endpoint. For example, a path efficiency of 1 indicates that the animal took a straight-line path to the target, whereas a path efficiency of 0.5 indicates that the animal traveled twice as far as the most direct path.

Time-to-target is calculated as the total time between the start tone and the time the mouse's head reaches the target.

Estimation of angle and direction from sensory information To quantify how well the animal could estimate the angle and direction of the target from each sensory modality, we isolated trials in which the velocity profiles had clearly identifiable bell-curves. A bell-curve shaped velocity profile was defined as one that had "onset" and "offset" points equal to baseline speed plus $0.5\sigma_v$, where σ_v is the standard deviation of the cropped velocity trace. Velocity on each trial was calculated as the difference in position of the animal normalized by the inverse of the camera frame rate (1/60 Hz$^-$1). This analysis includes trials in which the mouse was moving when the go cue sounded, slowed down to identify the target location based on the available sensory information, and then resumed moving. On these trials, we used the first sub-movement following the first pause to assess decoding of θ and of δ.

6 Acknowledgments

The work described here was supported by NSF HDR grant 2117997, NIH T-32 grant 016853-06 for Purdue University's Interdisciplinary Training Program in Auditory Neuroscience, and a grant from the Indiana CTSI Traumatic Spinal Cord & Brain Injury Research Program.

References

[1] Benoit P. Delhaye, Katie H. Long, and Sliman J. Bensmaia. "Neural basis of touch and proprioception". In: *Compr Physiol.* 8.4 (2018), pp. 1575–1602.

[2] G. H. Recanzone et al. "Topographic reorganization of the hand representation in cortical area 3b of owl monkeys trained in a frequency-discrimination task". In: *Journal of Neurophysiology* 67.5 (1992), pp. 1031–1056.

[3] Solaiman Shokur et al. "Expanding the primate body schema in sensorimotor cortex by virtual touches of an avatar". In: *Proceedings of the National Academy of Sciences of the United States of America* 110.37 (2013), pp. 15121–15126.

[4] Angelo Maravita and Atsushi Iriki. "Tools for the body (schema)". In: *Trends in Cognitive Sciences* 8.2 (2004), pp. 79–86.

[5] G H Recanzone, M M Merzenich, and H R Dinse. "Expansion of the cortical representation of a specific skin field in primary somatosensory cortex by intracortical microstimulation." In: *Cerebral cortex (New York, N.Y. : 1991)* 2.3 (1992), pp. 181–96.

[6] James M. Rebesco et al. "Rewiring neural interactions by micro-stimulation". In: *Frontiers in Systems Neuroscience* 4.August (2010), pp. 1–15.

[7] Andrew Jackson, Jaideep Mavoori, and Eberhard E Fetz. "Long-term motor cortex plasticity induced by an electronic neural implant." In: *Nature* 444.7115 (2006), pp. 56–60.

[8] S. N. Flesher et al. "Intracortical microstimulation of human somatosensory cortex". In: *Science Translational Medicine* 8.361 (2016), 361ra141–361ra141.

[9] Christopher L. Hughes et al. "Perception of microstimulation frequency in human somatosensory cortex". In: *eLife* 10 (2021), pp. 1–19.

[10] Kevin J. Otto, Patrick J. Rousche, and Daryl R. Kipke. "Microstimulation in auditory cortex provides a substrate for detailed behaviors". In: *Hearing Research* 210.1-2 (2005), pp. 112–117.

[11] Giacomo Valle et al. "Tactile Edges and Motion Via Patterned Microstimulation of the Human Cortex". In: *Science* 387 (2025), pp. 315–322.

[12] Ranulfo Romo et al. "Somatosensory discrimination based on cortical microstimulation". In: *Nature* 292.March (1998), pp. 387–390.

[13] Léo Pio-Lopez, Romanos Poulkouras, and Damien Depannemaecker. "Visual cortical prosthesis: an electrical perspective". In: *Journal of Medical Engineering and Technology* 45.5 (2021), pp. 394–407.

[14] Xing Chen et al. "Shape perception via a high-channel-count neuroprosthesis in monkey visual cortex". In: *Science* 370.6521 (2020), pp. 1191–1196.

[15] G. Risso et al. "Optimal integration of intraneural somatosensory feedback with visual information: a single-case study". In: *Scientific Reports* 9.1 (2019), pp. 1–10.

[16] Roy Lycke et al. "Low-threshold, high-resolution, chronically stable intracortical microstimulation by ultraflexible electrodes". In: *Cell Reports* 42.6 (2023), p. 112554.

[17] Amy M. Ni and J. H R Maunsell. "Microstimulation Reveals Limits in Detecting Different Signals from a Local Cortical Region". In: *Current Biology* 20.9 (2010), pp. 824–828. eprint: `NIHMS150003`.

[18] Eric E. Thomson, Rafael Carra, and Miguel A.L. Nicolelis. "Perceiving invisible light through a somatosensory cortical prosthesis". In: *Nature Communications* 4 (2013), p. 1482. eprint: `NIHMS150003`.

[19] Eric E. Thomson et al. "Cortical neuroprosthesis merges visible and invisible light without impairing native sensory function". In: *eNeuro* 4.6 (2017), pp. 1–17.

[20] Joseph E. O'Doherty et al. "Creating a neuroprosthesis for active tactile exploration of textures". In: *Proceedings of the National Academy of Sciences of the United States of America* 116.43 (2019), pp. 21821–21827.

[21] Maria C Dadarlat. "Artificial Sensory Feedback for Neural Prostheses". PhD thesis. University of California, San Francisco, 2014, pp. 1078–1085.

[22] Maria C. Dadarlat and Philip N. Sabes. "Encoding and Decoding of Multi-Channel ICMS in Macaque Somatosensory Cortex". In: *IEEE Transactions on Haptics* 9.4 (2016), pp. 508–514.

[23] Kevin A. Mazurek and Marc H. Schieber. "Injecting Instructions into Premotor Cortex". In: *Neuron* 96.6 (2017), 1282–1289.e4.

[24] N A Fitzsimmons et al. "Primate Reaching Cued by Multichannel Spatiotemporal Cortical Microstimulation". In: *Journal of Neuroscience* 27.21 (2007), p. 5593.

[25] Amy L. Orsborn et al. "Closed-loop decoder adaptation shapes neural plasticity for skillful neuroprosthetic control". In: *Neuron* 82.6 (2014), pp. 1380–1393.

[26] Richard A. Andersen, Tyson Aflalo, and Spencer Kellis. "From thought to action: The brain-machine interface in posterior parietal cortex". In: *Proceedings of the National Academy of Sciences of the United States of America* 116.52 (2019), pp. 26274–26279.

[27] Sliman J. Bensmaia and Lee E. Miller. "Restoring sensorimotor function through intracortical interfaces: Progress and looming challenges". In: *Nature Reviews Neuroscience* 15.5 (2014), pp. 313–325.

[28] Chethan Pandarinath and Sliman J Bensmaia. "The science and engineering behind sensitized brain-controlled bionic hands". In: *Physiological Reviews* (2021).

[29] Maria C Dadarlat, Ryan A Canfield, and Amy L Orsborn. "Neural Plasticity in Sensorimotor Brain-Machine Interfaces". In: *Annual Review of Biomedical Engineering* 15.2 (2023), pp. 51–76.

[30] Philip N. Sabes. "Sensory integration for reaching. Models of optimality in the context of behavior and the underlying neural circuits". In: *Progress in Brain Research* 191 (2011), pp. 195–209.

[31] Marc O Ernst and Martin S Banks. "Humans integrate visual and haptic information in a statistically optimal fashion." In: *Nature* 415.6870 (2002), pp. 429–433. eprint: `NIHMS150003`.

[32] Barry E Stein and Terrence R Stanford. "Multisensory integration: current issues from the perspective of the single neuron." In: *Nature reviews. Neuroscience* 9.4 (2008), pp. 255–266.

[33] M J Prud'homme and J F Kalaska. "Proprioceptive activity in primate primary somatosensory cortex during active arm reaching movements." In: *Journal of neurophysiology* 72.5 (1994), pp. 2280–301.

[34] Ignacio Alonso et al. "Peripersonal encoding of forelimb proprioception in the mouse somatosensory cortex". In: *Nature Communications* 14 (2023), p. 1866.

[35] Seungbin Park, Megan H. Lipton, and Maria C. Dadarlat. "Population-level encoding of somatosensation in mouse sensorimotor cortex". In: *bioRxiv* (2025). eprint: `https://www.biorxiv.org/content/early/2025/01/21/2025.01.21.634118.full.pdf`.

[36] Stephanie Niklaus et al. "Challenging a myth and misconception: Red-light vision in rats". In: *Animals* 10.3 (2020), pp. 1–14.

[37] Gary A Kane, Jonny L Saunders, and Alexander Mathis. "Real-time, low-latency closed-loop feedback using markerless posture tracking". In: *eLife* 9 (2021), e61909.

[38] Mark H Histed, Vincent Bonin, and R Clay Reid. "Direct activation of sparse, distributed populations of cortical neurons by electrical microstimulation." In: *Neuron* 63.4 (2009), pp. 508–22.

[39] Nicholas J. Michelson et al. "Calcium activation of cortical neurons by continuous electrical stimulation: Frequency dependence, temporal fidelity, and activation density". In: *Journal of Neuroscience Research* 97.5 (2019), pp. 620–638.

[40] Maria C. Dadarlat, Yujiao Jennifer Sun, and Michael P. Stryker. "Activity-dependent recruitment of inhibition and excitation in the awake mammalian cortex during electrical stimulation". In: *Neuron* 112.5 (2024), 821–834.e4.

[41] Maria C. Dadarlat, Yujiao Sun, and Michael P. Stryker. "Widespread activation of awake mouse cortex by electrical stimulation". In: *International IEEE/EMBS Conference on Neural Engineering, NER*. Vol. 2019-March. 2019, pp. 1113–1117.

[42] Kevin C Stieger et al. "Intracortical microstimulation pulse waveform and frequency recruits distinct spatiotemporal patterns of cortical neuron and neuropil activation". In: *Journal of Neural Engineering* 19.2 (2022), p. 026024.

[43] Christopher P. Burgess et al. "High-Yield Methods for Accurate Two-Alternative Visual Psychophysics in Head-Fixed Mice". In: *Cell Reports* 20.10 (2017), pp. 2513–2524.

[44] Maria C. Dadarlat, Joseph E. O'Doherty, and Philip N. Sabes. "A learning-based approach to artificial sensory feedback leads to optimal integration". In: *Nature Neuroscience* 18.1 (2015), pp. 138–144.

[45] Isabelle A. Rosenthal et al. "Visual context affects the perceived timing of tactile sensations elicited through intra-cortical microstimulation". In: *bioRxiv* (2024). eprint: `https://www.biorxiv.org/content/early/2024/05/14/2024.05.13.593529.full.pdf`.

[46] K. Novak, L. Miller, and J. Houk. "The use of overlapping submovements in the control of rapid hand movements". In: *Experimental Brain Research* 144.3 (2002), pp. 351–364.

[47] Jason M. Samonds, Veronica Choi, and Nicholas J. Priebe. "Mice discriminate stereoscopic surfaces without fixating in depth". In: *Journal of Neuroscience* 39.41 (2019), pp. 8024–8037.

[48] Joseph G. Makin, Matthew R. Fellows, and Philip N. Sabes. "Learning Multisensory Integration and Coordinate Transformation via Density Estimation". In: *PLoS Computational Biology* 9.4 (2013), e1003035.

[49] Edwin M. Maynard, Craig T. Nordhausen, and Richard A. Normann. "The Utah Intracortical Electrode Array: A recording structure for potential brain-computer interfaces". In: *Electroencephalography and Clinical Neurophysiology* 102.3 (1997), pp. 228–239.

[50] Konstantin Hartmann et al. "Embedding a panoramic representation of infrared light in the adult rat somatosensory cortex through a sensory neuroprosthesis". In: *Journal of Neuroscience* 36.8 (2016), pp. 2406–2424.

[51] Sanjiv K. Talwar et al. "Rat navigation guided by remote control". In: *Nature* 417.6884 (2002), pp. 37–38.

[52] Andrew G. Richardson et al. "Learning active sensing strategies using a sensory brain–machine interface". In: *Proceedings of the National Academy of Sciences* 116.35 (2019), p. 201909953.

[53] Patrick T. Sadtler et al. "Neural constraints on learning". In: *Nature* 512.7515 (2014), pp. 423–426.

[54] Matthew D Golub et al. "Learning by neural reassociation". In: *Nature Neuroscience* 21.April (2018).

[55] Emily R Oby et al. "New neural activity patterns emerge with long-term learning". In: *Proceedings of the National Academy of Sciences of the United States of America* 116.30 (2019), pp. 15210–15215.

[56] John S Choi et al. "Eliciting naturalistic cortical responses with a sensory prosthesis via optimized microstimulation". In: *Journal of Neural Engineering* 13.5 (2016), p. 056007.

[57] Karthik Kumaravelu et al. "A comprehensive model-based framework for optimal design of biomimetic patterns of electrical stimulation for prosthetic sensation". In: *Journal of Neural Engineering* 17.4 (2020), p. 046045.

[58] Christopher Hughes and Takashi Kozai. "Dynamic amplitude modulation of microstimulation evokes biomimetic onset and offset transients and reduces depression of evoked calcium responses in sensory cortices". In: *Brain Stimulation* 16 (2023), pp. 939–965.

[59] Tucker Tomlinson and Lee E Miller. "Toward a Proprioceptive Neural Interface That Mimics Natural Cortical Activity". In: *Adv Exp Med Biol.* 957 (2016), pp. 367–388.

[60] Jacob L. Segil et al. "Combination of Simultaneous Artificial Sensory Percepts to Identify Prosthetic Hand Postures: A Case Study". In: *Scientific Reports* 10.1 (2020), pp. 1–15.

[61] Ivana Cuberovic et al. "Learning of Artificial Sensation Through Long-Term Home Use of a Sensory-Enabled Prosthesis". In: *Frontiers in Neuroscience* 13.August (2019), pp. 1–24.

[62] Anne E. Urai et al. "Citric acid water as an alternative to water restriction for high-yield mouse behavior". In: *eNeuro* 8.1 (2021), pp. 1–8.